NMR LOGGING OF NATURAL GAS RESERVOIRS

R. Akkurt, SPWLA, Shell Offshore Inc., New Orleans, LA,
H. J. Vinegar, SPWLA, Shell Development Co., Houston, TX,
P. N. Tutunjian, Shell Development Co., Houston, TX,
A. J. Guillory, SPWLA, Shell Offshore Inc., New Orleans, LA.

Abstract

The phenomenon causing reduced NMR porosities in gas reservoirs, the so called "gas effect", has lately become a subject of great interest in the petrophysical community. Contrary to the industry wide belief, NMR logging tools can detect gas provided that the pulse sequences are chosen properly and that the logging tool has adequate depth-of-investigation. Furthermore, gradient-based logging tools such as the MRIL-C can be used to unambiguously identify the gas phase in the reservoir. Failure to recognize gas may result in gas being misinterpreted as bound fluid, which in turn may result in excessively high irreducible water saturations and incorrect permeability estimates.

The NMR properties of gas are quite different from those of water and oil under typical reservoir conditions and this can be used to quantify the gas phase in a reservoir. A new NMR-only interpretation approach based on this principle, called the *Differential Spectrum Method* (DSM), has been developed and successfully tested in the Gulf of Mexico. This method utilizes properly selected NMR pulse sequences and does not require resistivity or other porosity logs. The DSM can be used in reservoirs containing gas and/or oil. Another technique exploiting the diffusion properties of gas, called the *Shifted Spectrum Method* (SSM), is also introduced.

Hydrocarbon saturations computed using the Differential and Shifted Spectrum Methods show very good agreement with those obtained conventionally. The methods are mineralogy independent and insensitive to clay bound water, and ideal for shaly sand applications.

Introduction

Figure 1 shows a set of open hole logs in a Gulf of Mexico gas reservoir. The zone of interest is easily recognized from the neutron-density crossover in the third track. Total porosity PHIT and total NMR porosity MPHI6 are shown in the fourth track.

The large reduction in NMR porosity compared to total porosity is an example of the so called *gas effect*. Contrary to the industry wide belief, NMR logs can detect the gas phase in a reservoir.

The first objective of this paper is to explain the gas effect and various other complications that arise as a result of the gas effect. The second objective is to introduce new interpretation methods that allow the quantification of hydrocarbon saturations from NMR logs alone, without using any other logs, in gas and/or oil reservoirs.

All the logs presented in this paper were acquired with the NUMAR MRIL-C tool. The MRIL-C is a gradient-based (17 *gauss/cm* fixed magnetic field gradient), dual-frequency tool (Chandler et al,1994). T_2 spectra were extracted from raw CPMG echo trains by breaking the total NMR signal $M(t)$ into 8 components, called bins,

$$M(t) = \sum_{i=1}^{8} a_i \, e^{-t/T_{2i}}, \qquad (1)$$

where a_i is the porosity associated with the ith bin (Prammer, 1994). Each bin is characterized by its fixed center transverse relaxation time T_{2i}, chosen such that $T_{2i} = 2^{i+1}\ ms$. Total NMR porosity ϕ_{nmr} is defined as the sum of the porosities in all bins,

$$\phi_{nmr} = \sum_{i=1}^{8} a_i. \qquad (2)$$

while the *capillary bound porosity* is defined as the sum of the porosities in the first three bins,

$$\phi_{cap} = \sum_{i=1}^{3} a_i, \qquad 4\ ms \leq T_{2i} \leq 16\ ms. \qquad (3)$$

The definition of ϕ_{cap} above is based on a T_2 cutoff of 30 ms which is valid for clastics. The T_2 cutoff for carbonates is about three times larger than in sandstones (Chang et al, 1994).

Total NMR porosity ϕ_{nmr} and capillary bound porosity ϕ_{cap} are also known as MPHI and MBVI. The difference of these quantities is the free fluid index MFFI.

NMR Properties of Natural Gas

Natural gas is composed predominantly of methane (CH_4) with small amounts of the lighter alkanes and some inerts. The NMR data presented here is for methane, but at a density corresponding to a slightly heavier gas mixture ($C_{1.1}H_{4.2}$).

The longitudinal relaxation time T_1 of natural gas is given by

$$\frac{1}{T_1} = \frac{1}{T_{1B}} + \frac{1}{T_{1S}}, \tag{4}$$

where subscripts B and S refer to bulk and surface relaxation, respectively. Gas is always a non-wetting phase in the pore space of the reservoir. Thus its T_1 is always that of the bulk gas, T_{1B}, since it is not shortened by surface relaxation. The T_1 of bulk methane depends only on its temperature and pressure, which are known accurately for most reservoirs.

Figures 2 and 3 show the density and hydrogen index (HI) as a function of pressure and temperature for the natural gas mixture described earlier (Schlumberger, 1987). Under the conditions most commonly found in gas production, the gas pressure varies from 2,000 to 10,000 *psi* and temperatures from 100 to 350°F, resulting in natural gas densities from 0.1 to 0.3 g/cc. The hydrogen index, HI, is proportional to the hydrogen density, and varies from 0.2 to 0.6 for the same pressure and temperature range. Although the HI of natural gas is less than that of water (1 for water and most oils), it is still quite large and can be measured with an appropriate NMR pulse sequence.

Figure 4 shows T_1 for methane as a function of temperature and pressure, extrapolated from measurements at the University of Amsterdam (Gerritsma et al, 1971). T_1 increases linearly with density at constant temperature and has the following temperature dependence on absolute temperature T:

$$ln(T_1) = A - B/T. \tag{5}$$

Equation (5) can be used to interpolate T_1 at other densities and temperatures.

Under typical reservoir conditions, the T_1 of supercritical methane is surprisingly short, varying from 3 to 6 s. For comparison, liquid methane has a T_1 of about 20 s below the critical point. The reason for the short T_1 in the low density supercritical and dilute gas regions is that gaseous methane is subject to an additional relaxation mechanism, spin-rotation relaxation, which is quenched in liquids. Liquids and dissolved gas relax primarily by dipole-dipole relaxation, where $T_1 \propto 1/viscosity$.

The transverse relaxation time T_2 in a magnetic field gradient is also affected by diffusion, in addition to bulk and surface relaxation, resulting in

$$\frac{1}{T_2} = \frac{1}{T_{2B}} + \frac{1}{T_{2S}} + \frac{1}{T_{2D}}. \tag{6}$$

T_{2D} for a CPMG sequence is

$$T_{2D} = \frac{3}{\gamma^2\, G^2\, D\, t_{cp}^2}, \tag{7}$$

where γ is the gyromagnetic ratio of ^1H (26,741 $radians/s/gauss$), G is the magnetic field gradient, D is the diffusion coefficient, and t_{cp} is half the interecho time. Since gas is in the short correlation time regime, $T_1 = T_{1B} \approx T_{2B}$. Surface relaxation is also negligible in Equation (6) because gas is always a non-wetting phase.

Figure 5 shows the unrestricted diffusion coefficient of methane as a function of temperature and pressure, extrapolated from Oosting and Trappeniers (1971), and also Dawson et al (1970). The range of D_0 is 70 to 150 x $10^{-5} cm^2/s$. Under typical reservoir conditions, methane diffuses at least an order of magnitude faster than water (D_0 is approximately 100 x $10^{-5} cm^2/s$ for gas, compared to 2.3 x $10^{-5} cm^2/s$ for water at room temperature).

Figure 6 shows T_{2D} of natural gas for MRIL-B and MRIL-C tools with the G and t_{cp} values as tabulated below.

Tool	G gauss/cm	t_{cp} ms
MRIL-C	17	0.6
MRIL-B	25	1.0

For the MRIL tools, the magnetic field gradient varies with temperature. For example, for the MRIL-C, G increases from 17 to 22 $gauss/cm$ while temperature changes from 70 to 300°F. The T_2 values shown in Figure 6 have been computed assuming a constant G. One should therefore account for the temperature dependence of G when using Equation (7).

It is clear from Figure 6 that natural gas would have a T_{2D} less than 10 ms for the MRIL-B, and would therefore be counted as capillary bound fluid. On the other hand, T_{2D} would be between 20 and 65 ms for the MRIL-C, and therefore may be counted partially as bound fluid.

Table 1 compares the NMR properties of brine, light oil, and natural gas for a typical Gulf of Mexico sandstone reservoir. The reservoir temperature in Table 1 is $200°F$, reservoir pressure is 4500 *psi*, oil viscosity at reservoir conditions is 0.2 *cp*, brine salinity is 120 *kppm NaCl* concentration, and G is 17 *gauss/cm*.

Table 1: **NMR Properties of Reservoir Fluids**

	T_1 ms	T_2 ms	HI	D_0 $\times 10^{-5}$ cm^2/s	D_0T_1 cm^2
brine	1 to 500	0.67 to 200	1	7.7	0.0077 to 4.0
oil	5000	460	1	7.9	40
gas	4400	40	0.38	100	440

This table shows that the T_1 of oil and natural gas may overlap despite a large T_2 contrast. One can also see from Table 1 that brine and oil may have overlapping D_0 or T_2, but distinctly separated T_1. These observations can be utilized to formulate pulse sequences that manipulate the similarities and contrasts in NMR properties of reservoir fluids. The Differential and Shifted Spectrum Methods, which are described later, are two examples of such formulations.

Errors in Irreducible Water Saturation and Permeability

Depending on D_0, G,and t_{cp}, the T_2 of the gas phase may get so short that all or some of the signal due to gas may appear in the MBVI window, resulting in excessively high MBVI values. The coupled effect of reduced porosity due to gas and shortened T_2s due to diffusion in a gradient may also result in incorrect permeability estimates derived from relations employing NMR logs.

There are two frequently used permeability models, the first based on the free fluid index MFFI, where

$$k = c\,\phi_{nmr}^4 \left[\frac{MFFI}{MBVI}\right]^2, \qquad (8)$$

and the second based on the logarithmic mean T_2 (Morriss et al, 1983), where

$$k = c'\,\phi_{nmr}^4\,T_{2L}^2. \qquad (9)$$

Both c and c' in Equations (8) and (9) are scaling constants. Although some variations of the above formulas exist in the literature, the general form of these relations are as above.

Permeability estimates may be extremely low when Equation (8) is employed in gas bearing zones with a gradient-based logging tool. Total NMR porosity ϕ_{nmr}, if uncorrected, will be too low due to the gas effect. MBVI, on the other hand, will be too high and MFFI too low, resulting in a very low permeability estimate. One can modify Equation (8) and use variations of this formula with porosities substituted from other logs. Such approaches may give better answers but remove the originality of the NMR-derived permeability application.

Equation (9) will also give erroneous results if used in place of Equation (8) in a gas-bearing zones with a gradient-based logging tool. In this case, ϕ_{nmr} will be too low due to the gas effect and T_{2L} will be much smaller than the true T_{2L} due to diffusion, again yielding a low estimate of permeability.

Invasion

Invasion is a source of concern in NMR logging due to the relatively shallow depth-of-investigation of NMR logging tools. The MRIL-C excites two shells centered on the borehole axis, with diameters of approximately 16 inches, (Chandler et al, 1994). The depth-of-investigation, therefore, varies with borehole size. For example, in a 10-inch borehole, the depth-of-investigation is about 3 inches, making the measurements sensitive to invasion.

Since the invading fluid replaces gas, this results in the reduction of the gas effect. In the extreme case of severe invasion, the logging tool may detect no gas. However, recent experiences in the Gulf of Mexico indicate that there is usually a reasonable amount of residual gas in the zone investigated by the MRIL-C, allowing at least the detection of gas by the tool, if not its quantification. Moreover, for oil-based muds, only a small amount of filtrate reaches the diameter-of-investigation of the MRIL-C.

The Differential Spectrum Method

Table 1 shows the interesting fact that light oil and natural gas may have overlapping T_1, but distinctly separated T_2 in the presence of a magnetic field gradient, allowing the separation of the gas phase from the liquid phase on the basis of diffusion properties. Similarly, Table 1 shows that brine and water may have overlapping D_0, but a large T_1 contrast, allow-

ing the separation of the two liquids on the basis of longitudinal relaxation properties.

The Differential Spectrum Method makes use of the observations above and is illustrated in Figure 7 for a sandstone reservoir containing brine, light oil and gas, using the NMR fluid properties given in Table 1. In the DSM, two logging passes are made with wait times τ_L and τ_S, such that $\tau_L \geq T_{1g}$ and $T_{1g} \geq \tau_S \geq 3T_{1w,max}$. For example, τ_L is 8 s and τ_S is 1.5 s. Due to the large T_1 contrast between the brine and the hydrocarbons, the water signal disappears when the two spectra are subtracted. Thus, the differential spectrum contains only hydrocarbon signals. The gas signal in Figure 7 is concentrated at about 40 ms and oil at about 460 ms.

The total signal for each phase must be corrected for HI and T_1 to obtain the pore volume occupied by that phase. Once the pore volumes associated with oil and gas phases are determined, the hydrocarbon saturation for each phase can be found by dividing the associated pore volume by corrected ϕ_{nmr}, or ϕ_T, to get effective or total saturations, respectively.

Note that the subtraction of the spectra also eliminates any clay bound water, making the DSM particularly useful in shaly sands. An analytical treatment of the DSM is included in Appendix A.

Figure 8 is an example of the application of the DSM in a gas reservoir. The T_2 spectra are gray scale T_2 histograms displayed versus depth. The spectrum in the 4th track is for $\tau_L = 6$ s, while the spectrum in the 5th track is for $\tau_S = 3$ s. Most of the signal is concentrated in the short bins, both in track 4 and 5, because the reservoir is at irreducible conditions ($T_{2w,max} \leq 32$ ms) and T_2 of gas is about 40 ms. Note the focused energy around the 32 and 64 ms bins in the differential spectrum due to gas. Also, note the absence of the brine signal in the differential spectrum in the shaly zone just below the gas. The well was drilled with an oil-based mud, but the absence of any signal in the 512 ms bin in the differential spectrum shows that there is no significant invasion (mud NMR properties were determined from laboratory measurements).

Figure 9 is an application of the DSM in an oil reservoir, also at irreducible conditions. In contrast to Figure 8, the longest bin contains strong signal, both for the $\tau_L = 8$ s and $\tau_S = 3$ s cases. The differential spectrum contains only the oil signal, at about 512 ms. Note the absence of any signal in the short bins, due to complete cancellation of the water signal.

This well was also drilled with an oil-based mud. One may question the origin of the signal in the differential spectrum, whether it is due to the oil-based mud filtrate or native oil. The signal in the differential spectrum is from native oil because following laboratory measurements of the mud, the wait times for the DSM were chosen such that the mud filtrate was fully polarized in both passes, resulting in full cancellation of the mud filtrate signal in the differential spectrum.

The ability distinguish the nature of the hydrocarbon fluids when drilling with oil-based muds is a powerful feature of NMR logging.

The Shifted Spectrum Method

Since surface relaxation is negligible for gas, Equations (6) and (7) can be combined to obtain the apparent T_2 for the gas phase as below:

$$\frac{1}{T_2} = \frac{1}{T_{2B}} + \frac{\gamma^2 G^2 t_{cp}^2 D}{3}. \quad (10)$$

By rearranging Equation (10),

$$\frac{1}{T_2} = \frac{1}{T_{2B}} [1 + \frac{\gamma^2 G^2 t_{cp}^2 D T_{2B}}{3}], \quad (11)$$

and recalling from earlier discussion that for a non-wetting phase

$$T_1 = T_{1B} \approx T_{2B}, \quad (12)$$

the following can be written for the signal due to the gas phase from a CPMG sequence,

$$M(t) = M_0(1 - e^{-\tau/T_1})\, e^{(-t/T_1)(1+\frac{\gamma^2 G^2 t_{cp}^2 D T_1}{3})}, \quad (13)$$

where τ is the wait time.

Given that the D_0T_1 of gas is an order of magnitude greater than oil, and two orders of magnitude greater than brine, one can see from Equation (13) that the already large DT_1 contrast of gas can be enhanced by increasing the interecho time $2t_{cp}$ in order to allow the separation of two fluids that overlap in T_1 (typical D_0T_1 of reservoir fluids can be seen in Table 1). The *Shifted Spectrum Method* (SSM) described below is an implementation of this concept.

The SSM is illustrated in Figures 10 and 11 for a gas reservoir at irreducible conditions, where $\phi_{cap} = 10$ $p.u.$, and $\phi_g = 20$ $p.u.$ The brine signal is equally distributed between 8 and 16 ms. The gas signal is centered at 40 ms (see Table 1).

The Shifted Spectrum Method requires the acquisition of two CPMG sequences both with wait time τ_L but different t_{cp}. The wait time is chosen such that $\tau_L > T_{1g}$. As an example, $\tau_L = 8$ s, $t_{cp} = 0.6$ ms in the first pass and $t_{cp} = 2.4$ ms in the second pass. Figure 10 shows the synthetic NMR decay curves for both passes. The solid curve

(labelled 'a') is for the short interecho time. One can see that the NMR signal decays much faster in the $t_{cp} = 2.4\ ms$ case (dashed curve labelled 'b') due to gas diffusion.

The corresponding T_2 spectra are shown in Figure 11. Only every fourth echo from the first pass has been included in the processing in order to eliminate T_2 bias. Also, the first two echoes from the two resulting CPMG sequences have been discarded. The solid curve (labelled 'a') is the T_2 spectrum for the short interecho time pass, where the 40 *ms* peak belongs to the gas phase. The second broader peak, centered about 12 *ms* is due to brine. Note that the increase in t_{cp} in the longer interecho time pass (labelled 'b') has *shifted* the gas spectrum below detectibility, leaving only the brine signal in the spectrum.

The SSM may be preferred over the DSM in shaly gas sands. The amount of signal in the differential spectrum may be very small when the DSM is used in a reservoir where the gas filled porosity and HI are low. This is particularly important when the signal-to-noise ratio (S/N) is lower.

Conclusions

NMR logging tools can detect natural gas and logs with properly chosen pulse sequences can be used to unambiguously measure the amount of gas-filled porosity.

The amount of reduction in NMR porosity depends on the reservoir properties and the pulse sequences used. The long T_1 and low hydrogen index of gas is the cause of the reduction in NMR porosity. The reduced NMR porosity, if not corrected, may result in very low permeability estimates. Also, because of the magnetic field gradient of commercially available logging tools, the T_2 of gas may be very short and signal originating from gas may be interpreted as capillary bound water, resulting in excessively high irreducible water saturations as well as extremely low permeability estimates. These phenomena may be complicated by invasion.

The different relaxation and diffusion properties of reservoir fluids can be exploited to determine the saturations of various phases. The Differential and Shifted Spectrum Methods are two implementations of this principle. The DSM allows a gradient-based NMR logging tool to determine the fluid properties of the hydrocarbon fluid in the reservoir.

The DSM and SSM do not have to be implemented in the form of two logging passes. Since the MRIL-C excites two different frequencies, the wait times or interecho times associated with each frequency may be set differently to implement these methods in a single logging pass. This approach does not suffer from depth shift problems and is operationally more efficient. However, the S/N of the logs must be considered before opting for this alternative. The two-pass approach is more likely to yield more robust T_2 estimates since for a dual-frequency tool, the S/N ratio is $\sqrt{2}$ times better than that of the multi-wait time single pass approach.

Due to the fact that clay bound water is not detected by the NMR logging tools, the DSM and SSM may be employed with more success in shaly sands with less effort since the method is free of the complications of resistivity-based interpretation. The SSM may be preferred over the DSM in shaly gas sands.

If the T_1 of brine is not short enough, as in carbonates, a small concentration of manganese ion can be added to the drilling mud (Horkowitz et al, 1995). This would extend the applicability of the DSM and SSM to carbonate lithologies.

Acknowledgements

The authors would like to thank their colleagues at Shell Offshore Inc. for sharing their data and knowledge of the fields, and management for allowing the publication of this work.

References

Akkurt, R., 1990, Effects of motion in pulsed NMR logging: Ph.D. thesis, Colorado School of Mines.

Chandler, R. N., Drack, E. D., Miller, M. N., and Prammer, M.G., 1994, Improved log quality with a dual-frequency pulsed NMR tool: Presented at the 69th Ann. Mtg., Society of Petroleum Engineers.

Chang, D., Vinegar, H. J., Morriss, C. E., and Straley, C., 1994, Effective porosity, producible fluid and permeability in carbonates from NMR logging: Presented at the 35th Ann. Mtg., Society of Professional Well Log Analysts, Paper A.

Dawson, R., Khory, F., and Kobayashi, R., 1970, Self-diffusion measurements in methane by pulsed nuclear magnetic resonance: AIChE Journal, Vol 16, No. 5, p.725-729.

Gerritsma, C. J., Oosting, P. H., and Trappeniers, N. J., 1971, Proton spin-lattice relaxation and

self-diffusion in methanes: II. Experimental results for proton spin-lattice relaxation times: Physica, **51**, 381-394.

Horkowitz, J. P., Vinegar, H. J., Hartman, D. E., Coates, G. R., and Clerke, E. A., 1995, Residual oil saturation measurements in carbonates with pulsed NMR Logs: Presented at the 36th Ann. Mtg., Society of Professional Well Log Analysts.

Morriss, C. E., MacInnis, J., Freedman, R., Smaardyk, J., Straley, C., Kenyon, W. E., Vinegar, H. J., and Tutunjian, P. N., 1993, Field test of an experimental pulsed nuclear magnetism tool: Presented at the 34th Ann. Mtg., Society of Professional Well Log Analysts.

Oosting, P. H., and Trappeniers, N. J., 1971, Proton spin-lattice relaxation and self-diffusion in methanes: IV. Self-diffusion in methanes: Physica, **51**, 418-431.

Prammer, M.G., 1994, NMR pore size distributions and permeability at the well site: Presented at the 69th Ann. Mtg., Society of Petroleum Engineers.

Schlumberger Educational Services, 1987, Log Interpretation Principles/ Applications: p. 45.

Authors

Ridvan Akkurt is a senior geophysicist with Shell Offshore Inc. in New Orleans, where he has worked in seismic data processing and petrophysics since joining Shell in 1991. Prior to Shell, Ridvan worked for Schlumberger in Africa as a wireline field engineer, and later in the US in research, and also for GSI in the Middle East as a field seismologist. He has a BS in Electrical Engineering from the Massachusetts Institute of Technology and a Ph D in Geophysics from the Colorado School of Mines. Akkurt is a member of SEG and SPWLA.

Harold J. Vinegar is a research advisor with Shell Exploration and Production Technology Company in Houston. Since joining the Shell Bellaire Research Center in 1976, his research interests have been in shaly sand evaluation, NMR logging, CT and NMR imaging, enhanced recovery processes and environmental remediation. He holds MA and Ph D degrees in physics from Harvard University and a BA from Columbia. He served as president and vice-president technology of the Society of Core Analysts. Harold is an associate editor for the Log Analyst and was coorganizer of the 1994 SPWLA Forum on Well Logging Applications of Nuclear Magnetic Resonance. He received the SPWLA Distinguished Technical Achievement Award in 1992.

Pierre Tutunjian is a senior research chemist at Shell Development Co. His research has been in the application of electron spin resonance and NMR spectroscopy and imaging techniques for products and exploration and production R&D. He holds a BA degree in chemistry from New York U. and a Ph D degree in physical chemistry from the Massachusetts Institute of Technology.

Abner Guillory is the Shelf Division Petrophysical Engineering Technical Specialist for Shell Offshore Inc. During his 20 years at Shell, he has had operational and supervisory assignments, in research and various operating divisions in the Gulf of Mexico. He has taught at Tulane University as an Adjunct Assistant Professor for two years. He is a member of SPWLA and SPE. He has served on the Board of Directors of SPWLA, and has been a technical editor for SPE. Guillory holds a BS degree in Physics from the University of Southwestern Louisana.

Appendix A

Defining $P(\tau, T_2)$ as the T_2 spectrum of a water-wet system obtained from a CPMG sequence with wait time τ, the following can be written for a three-phase system containing water, gas and oil:

$$\begin{aligned} P(\tau,T_2) = \quad & \alpha(\tau,T_{1w})P_W(T_2) \\ & +\alpha(\tau,T_{1g})P_G(T_2) \\ & +\alpha(\tau,T_{1o})P_O(T_2). \end{aligned} \tag{A1}$$

$P_W(T_2)$,$P_G(T_2)$ and $P_O(T_2)$ are the T_2 spectra for water, gas and oil, respectively, in the limit as τ approaches infinity, i.e.,

$$P(T_2) = \lim_{\tau\to\infty} P(\tau,T_2). \tag{A2}$$

The porosity due to each component is given by

$$\phi_w = \int P_W(T_2)\, dT_2, \tag{A3}$$

$$\phi_g = \frac{1}{HI_g}\int P_G(T_2)\, dT_2, \tag{A4}$$

$$\phi_o = \int P_O(T_2)\, dT_2, \tag{A5}$$

where HI_g is the hydrogen index of the gas. The hydrogen index for oil and water are assumed to be 1.

The polarization factor α in Equation (A1) accounts for incomplete polarization due to finite duration τ:

$$\alpha(\tau, T_1) = 1 - e^{-\tau/T_1}. \quad \text{(A6)}$$

The definition of α above is valid for stationary measurements. In general, α is a function of sonde design (for example the length of the rf antenna) and logging speed (Akkurt, 1990).

The spectra in Equation (A1) have limited ranges:

$$P_W(T_2) \geq 0 \ \ for \ \ T_2 \in [0, T_{2w,max}], \quad \text{(A7)}$$
$$P_G(T_2) \geq 0 \ \ for \ \ T_2 \in [T_{2D}, T_{2D'}], \quad \text{(A8)}$$
$$P_O(T_2) \geq 0 \ \ for \ \ T_2 \in [T_{1o} - \xi, T_{1o} + \xi]. \quad \text{(A9)}$$

$T_{2w,max}$ in Equation (A7) is the longest spin-spin relaxation time contributing to $P_W(T_2)$. The lower and upper bounds in Equation (A8) are controlled by the molecular diffusion of gas. The lower bound T_{2D} corresponds to the case when unrestricted diffusion takes place,

$$T_{2D} = \frac{3}{\gamma^2 G^2 D_0 t_{cp}^2}, \quad \text{(A10)}$$

where γ is the gyromagnetic ratio for the proton, G is the magnetic field gradient, D_0 is the unrestricted diffusion coefficient for gas, and t_{cp} is the inter echo time. While the lower bound is governed by unrestricted diffusion, the upper bound is affected by restricted diffusion. D'/D_0, the ratio of restricted diffusion coefficient to unrestricted diffusion coefficient, approaches the reciprocal of tortuosity in the limit:

$$\frac{D'}{D_0} = \frac{1}{\Gamma} = \frac{1}{F\phi}, \quad \text{(A11)}$$

where Γ is the tortuosity, and F is the formation factor in Archie Equation. The upper bound $T_{2D'}$ is obtained by computing D' from Equation (A11) and substituting its value for D_0 in Equation (A10). The T_2 range for the oil phase is given in terms of T_1 in Equation (A9), since water is the wetting phase and $T_{1o} \approx T_{2o}$. Also, $\xi \ll T_{1o}$ in Equation (A9). For typical reservoir temperatures and pressures, and oil viscosities, the following is true:

$$0 < T_{2D} < T_{2D'} < T_{2w,max} \ll T_{1g}, T_{1o}. \quad \text{(A12)}$$

Consider two logging passes, one acquired with a *long* wait time τ_L, and the other with a *short* wait time τ_S, where $\tau_L > \tau_S$. The wait times are chosen so that

$$\alpha(\tau_L, T_{1w}) - \alpha(\tau_S, T_{1w}) \approx 0, \quad \text{(A13)}$$
$$\alpha(\tau_L, T_{1g}) - \alpha(\tau_S, T_{1g}) > 0, \quad \text{(A14)}$$
$$\alpha(\tau_L, T_{1o}) - \alpha(\tau_S, T_{1o}) > 0. \quad \text{(A15)}$$

A particular solution satisfying the conditions given above is

$$\tau_L \approx 2\max(T_{1g}, T_{1o}), \quad \text{(A16)}$$
$$\min(T_{1g}, T_{1o}) \geq \tau_S \geq 3T_{1w,max}. \quad \text{(A17)}$$

Under these circumstances, the differential spectrum $\Delta P(T_2)$, which is the difference of $P(\tau_L, T_2)$ and $P(\tau_S, T_2)$, becomes

$$\Delta P(T_2) = [\alpha(\tau_L, T_{1g}) - \alpha(\tau_S, T_{1g})]\, P_G(T_2) \quad \text{(A18)}$$
$$+ [\alpha(\tau_L, T_{1o}) - \alpha(\tau_S, T_{1o})]\, P_O(T_2). \quad \text{(A19)}$$

Note that the water spectrum is absent in the above equations because of the constraint given in Equation (A13). Since the oil and gas spectra are mutually exclusive as shown in Equation (A12), the gas and oil filled porosities are computed with the aid of Equations (A4) and (A5) as follows:

$$\phi_g = \frac{\int_{T_{2D}}^{T_{2D'}} \Delta P(T_2)\, dT_2}{HI_g\ [\alpha(\tau_L, T_{1g}) - \alpha(\tau_S, T_{1g})]}, \quad \text{(A20)}$$

$$\phi_o = \frac{\int_{T_{1o}-\xi}^{T_{1o}+\xi} \Delta P(T_2)\, dT_2}{[\alpha(\tau_L, T_{1o}) - \alpha(\tau_S, T_{1o})]}. \quad \text{(A21)}$$

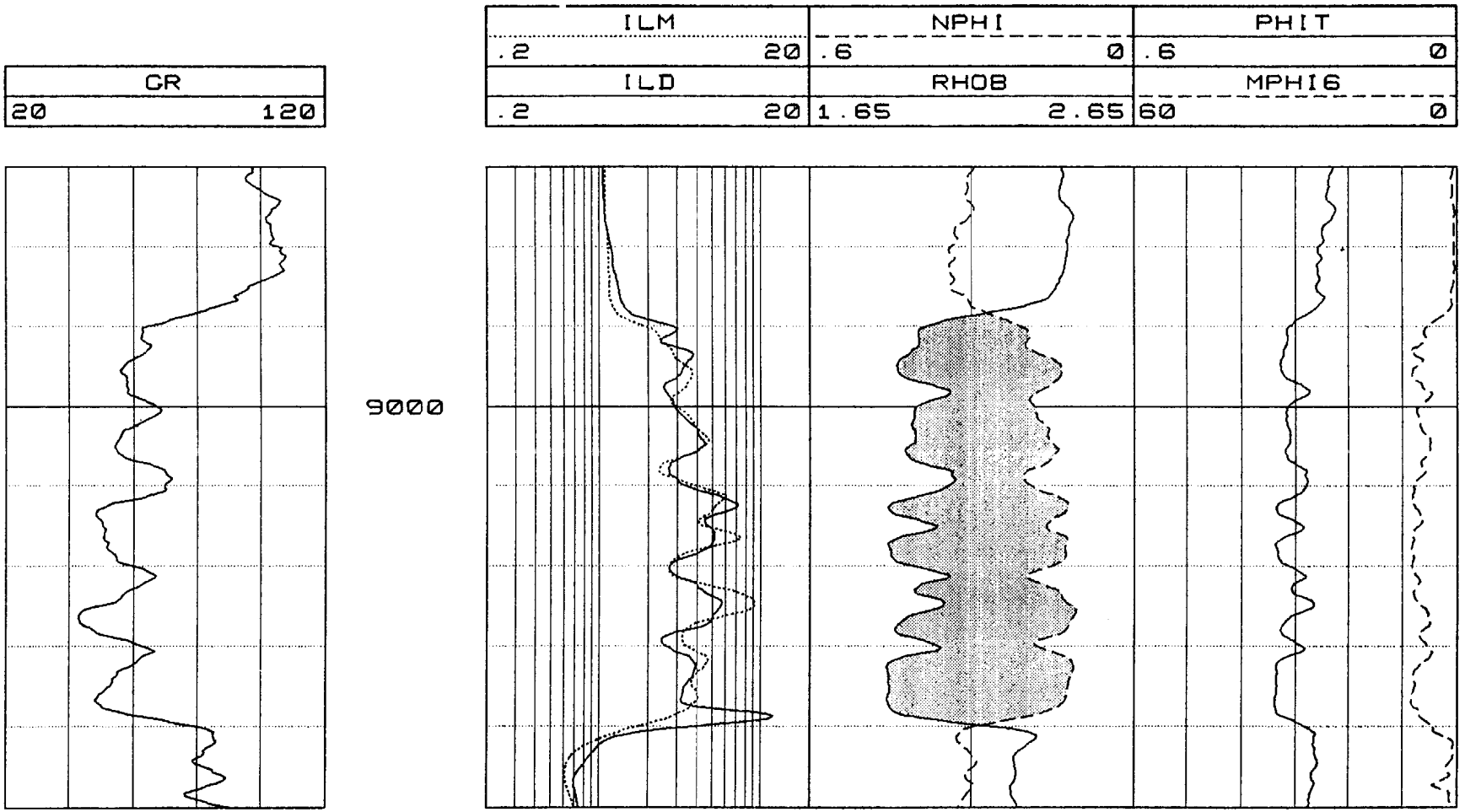

Figure 1: Open hole logs in gas bearing zone. Gamma ray is in the first track, medium and deep induction in the second, thermal neutron and bulk density in the third (in sandstone scales), total porosity and NMR porosity in the fourth track. Depth lines occur at every 10 feet. The NMR log was acquired with a wait time of 6 seconds. The large reduction in NMR porosity compared to total porosity is an example of the *gas effect*.

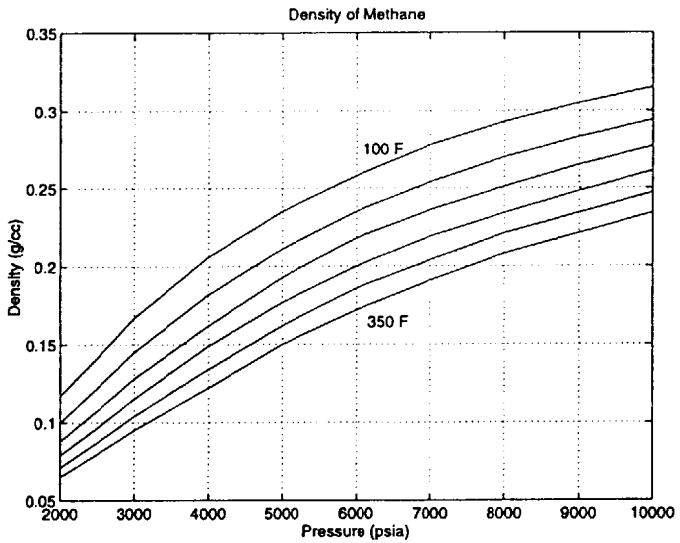

Figure 2: Density of methane ($C_{1\,1}H_{4\,2}$). Temperature increases from top to bottom at 50° F increments.

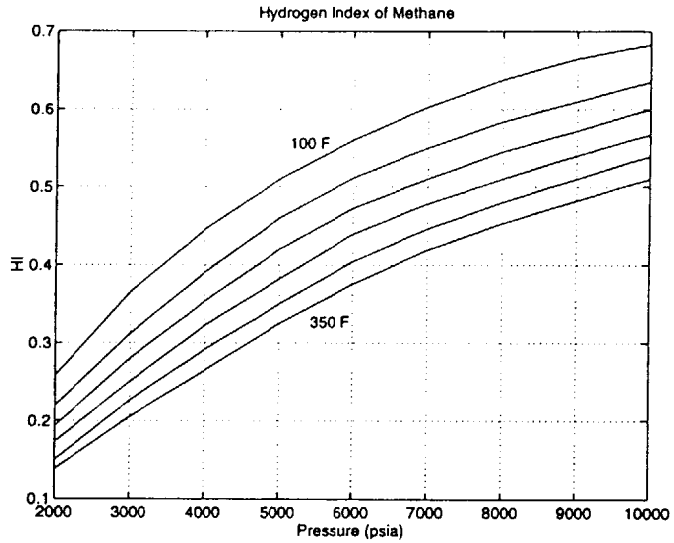

Figure 3: Hydrogen index of methane ($C_{1\,1}H_{4\,2}$). Temperature increases from top to bottom at 50° F increments. The HI of methane, although small compared to that of water, is still large and can be measured by appropriately selected pulse sequences

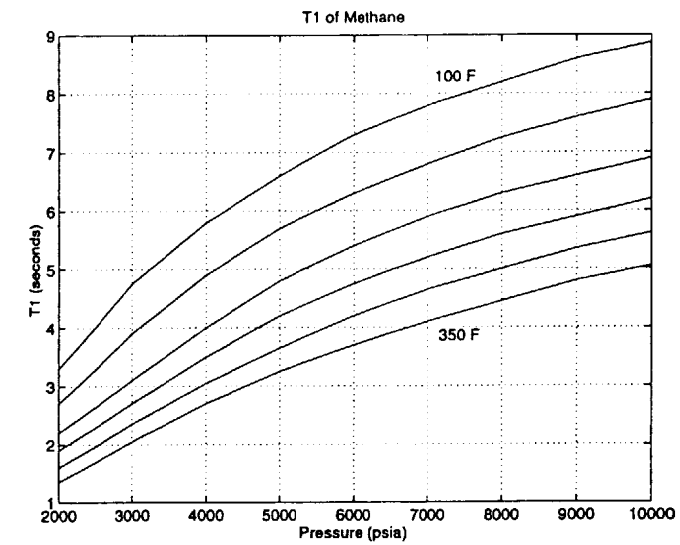

Figure 4: T_1 of methane. Temperature increases from top to bottom at 50° F increments.

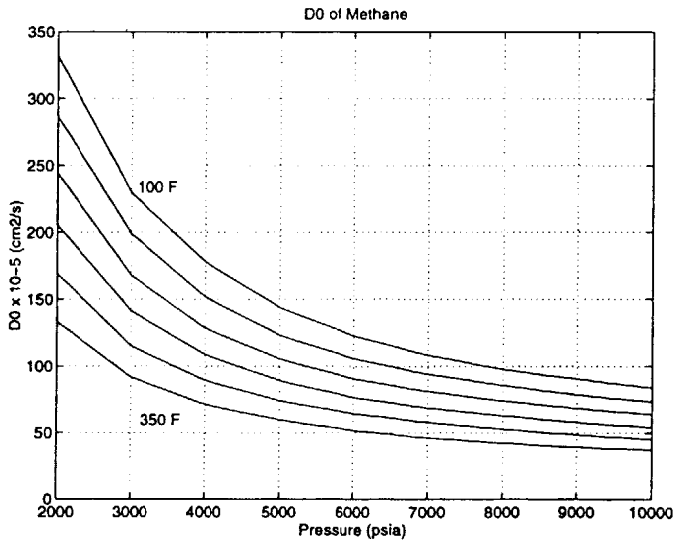

Figure 5 Unrestricted diffusion coefficient of methane. Temperature increases from top to bottom at 50° F increments.

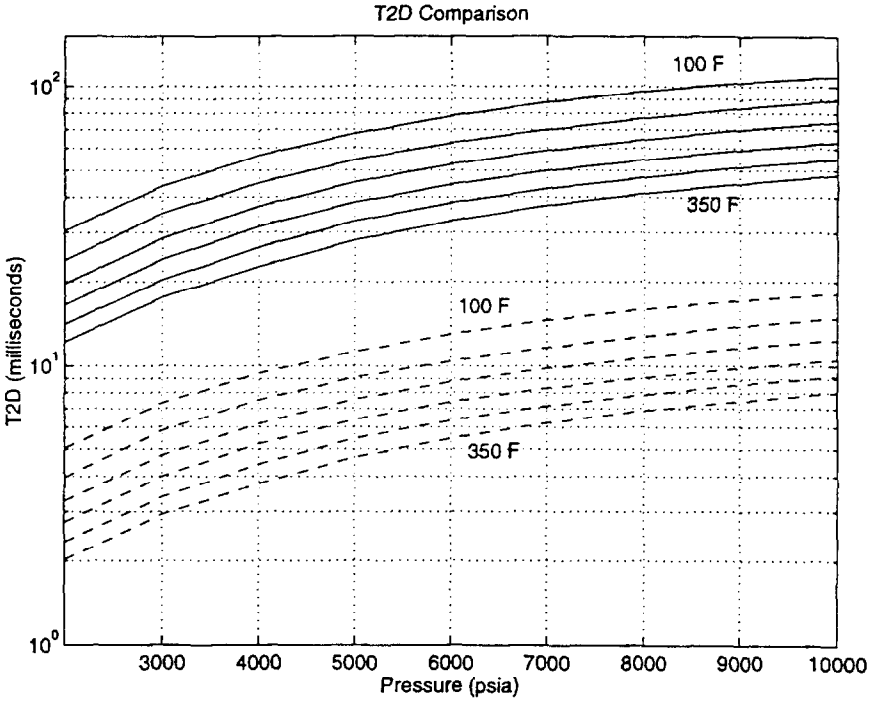

Figure 6: T_{2D} of natural gas, for MRIL-B (dashed) and MRIL-C (solid) tools. $G = 17$ *gauss/cm*, $t_{cp} = 0.6$ *ms* for MRIL-C, and $G = 25$ *gauss/cm*, $t_{cp} = 1.0$ *ms* for MRIL-C. G is assumed to be temperature independent in this figure.

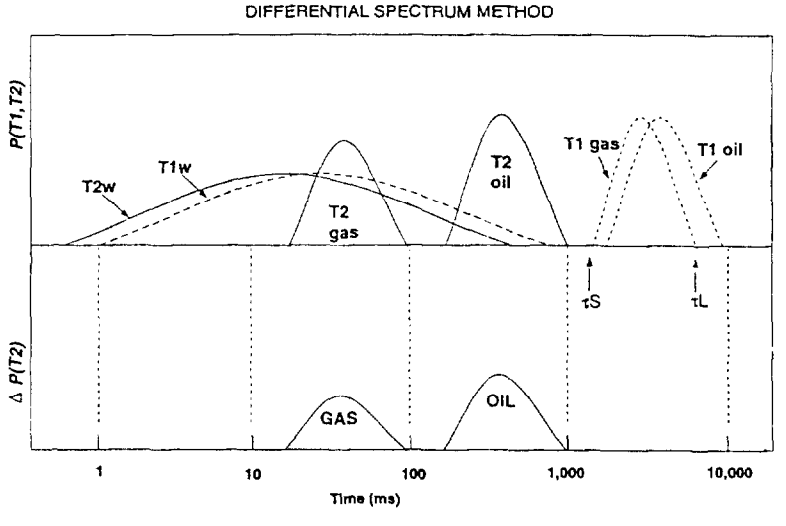

Figure 7: Schematic illustrating the *Differential Spectrum Method* (DSM) in a typical Gulf of Mexico sandstone reservoir. The brine, oil, and gas properties are listed in Table 1. In the DSM, two logging passes are made with short and long wait times, τ_S and τ_L, respectively. The difference spectrum consists of only hydrocarbon signals with oil and gas resolved based on differences in diffusion coefficient.

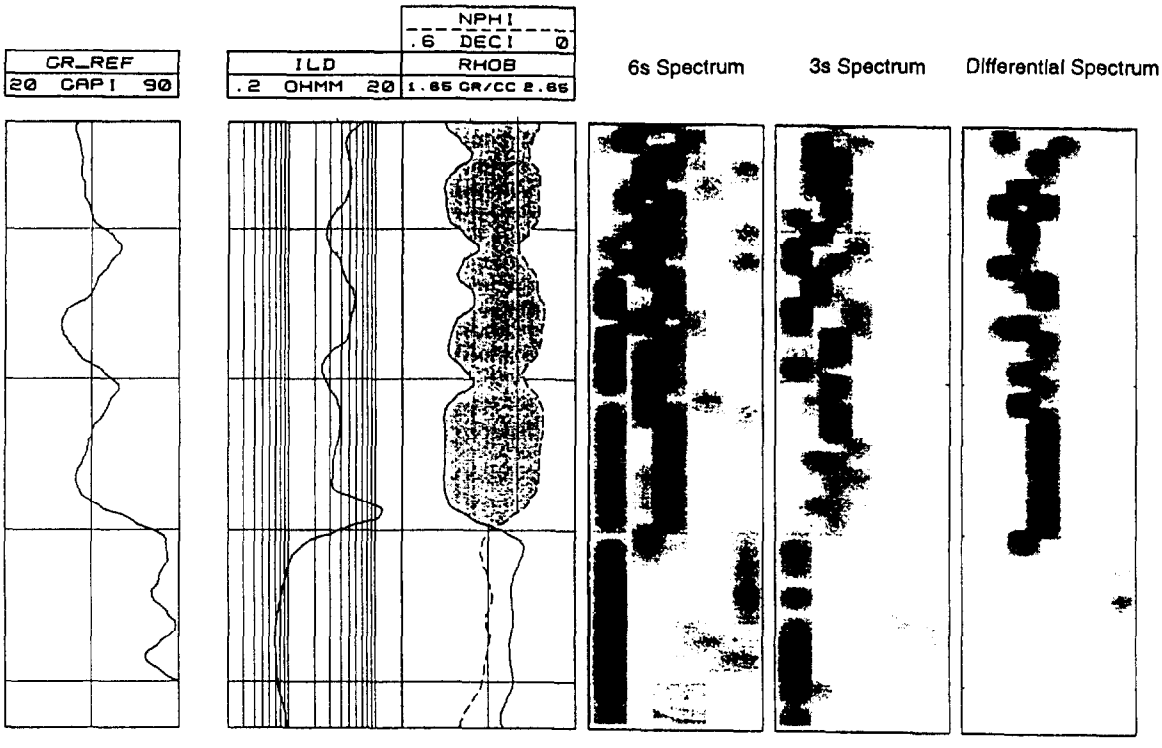

Figure 8: Open hole logs and T_2 spectra in a 40 feet gas bearing zone. GR is in the 1st track, induction resistivity in the 2nd, thermal neutron and bulk density in the 3rd, T_2 image for $\tau_L = 6$ *s* in the 4th, T_2 image for $\tau_S = 3$ *s* in the 5th, and the differential spectrum in the 6th track. Neutron density crossover has been shaded in gray. T_2 increases from 4 *ms* on the right to 512 *ms* on the left. The signal in the differential spectrum is concentrated around the 32 and 64 *ms* bins. Note the absence of signal in the shaly zone, just below the gas bearing sand.

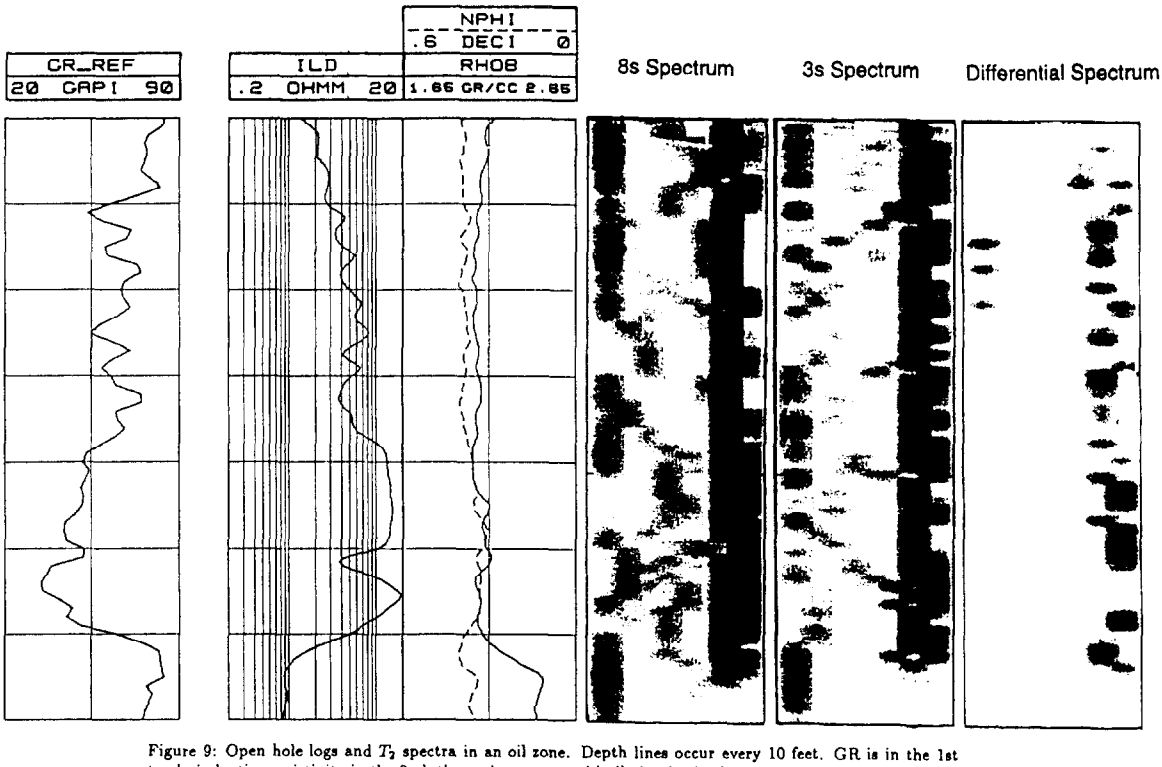

Figure 9: Open hole logs and T_2 spectra in an oil zone. Depth lines occur every 10 feet. GR is in the 1st track, induction resistivity in the 2nd, thermal neutron and bulk density in the 3rd, T_2 image for $\tau_L = 8$ *s* in the 4th, T_2 image for $\tau_S = 3$ *s* in the 5th, and the differential spectrum in the 6th track. T_2 increases from 4 *ms* on the right to 512 *ms* on the left. The signal in the differential spectrum is concentrated in the 512 *ms* bin.

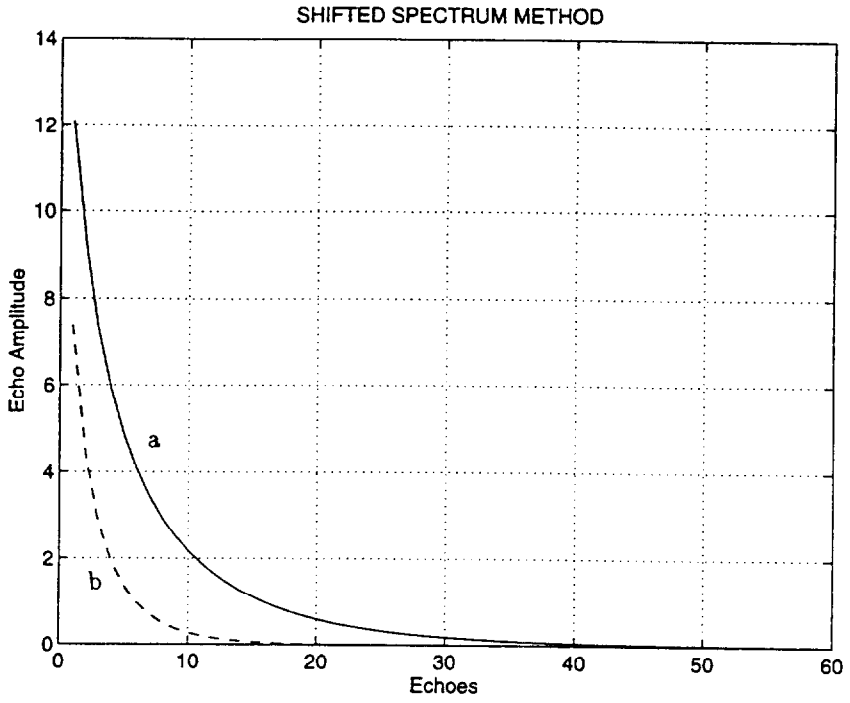

Figure 10: Synthetic T_2 decay curves illustrating the *Shifted Spectrum Method* in a gas bearing zone at irreducible water saturation. $\phi_g = 20$ *p.u.* and $\phi_{cap} = 10$ *p.u.* NMR properties for the gas phase are given in Table 1. The solid decay curved labelled 'a' is for the short interecho time, where $t_{cp} = 0.6$ *ms*. The dashed curve (labelled 'b') is for the $t_{cp} = 2.4$ *ms* case.

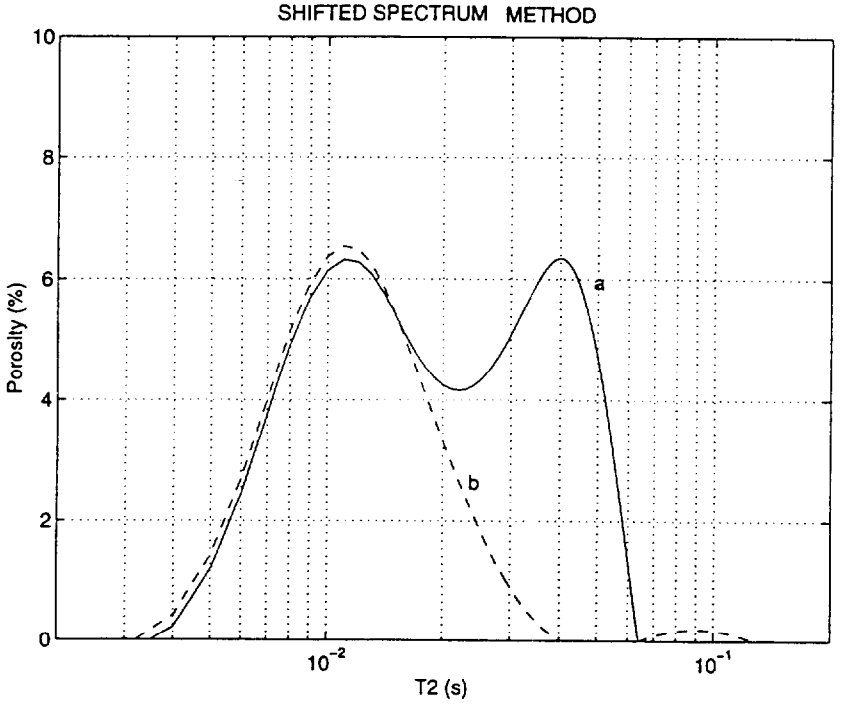

Figure 11: T_2 spectra obtained from the inversion of the synthetic echo trains shown in the previous figure. The solid spectrum (labelled 'a') corresponds to the $t_{cp} = 0.6$ *ms* case while the dashed spectrum (labelled 'b') corresponds to the $t_{cp} = 2.4$ *ms* case. Spectrum 'a' contains both gas and brine, where the peak at 40 *ms* is due to gas. The signal from gas is *shifted* out below detectibility in spectrum 'b' where the only peak is for the brine.